Sensors & Actuators: B. Chemical 295 (2019) 1–6

Contents lists available at ScienceDirect

Sensors and Actuators B: Chemical

journal homepage: www.elsevier.com/locate/snb

Turn-on fluorescence detection of β-glucuronidase using RhB@MOF-5 as an ultrasensitive nanoprobe

Lan Guo[a], Yuan Liu[b], Rongmei Kong[a], Guang Chen[a], Hao Wang[a], Xiuli Wang[a], Lian Xia[a,*], Fengli Qu[a,*]

[a] Key Laboratory of Life-Organic Analysis of Shandong Province, Qufu Normal University, Qufu, PR China
[b] Center for Research at Bio/Nano Interface, Department of Chemistry and Department of Physiology and Functional Genomics, Health Cancer Center, UF Genetics Institute and McKnight Brain Institute, University of Florida, Gainesville, FL, 32611-7200, United States

ARTICLE INFO

Keywords:
β-glucuronidase
RhB@MOF-5
Inner filter effect
Metal organic framework

ABSTRACT

β-Glucuronidase (β-GCU) is closely related to the occurrence of multiple diseases, and it has been applied as a biomarker and therapeutic target in clinical diagnosis. However, reliable methods with high selectivity and sensitivity for monitoring β-GCU are still lacked. Herein, we designed a novel fluorescent nanoprobe, rhodamine B encapsulated MOF-5 (RhB@MOF-5) for the first time, to detect β-GCU through the synergistic effect of inner filter effect (IFE) and static quenching effect (SQE) by employing 4-nitrophenyl-β-D-glucuronide (PNPG) as the substrate. After encapsulating into MOF-5, the fluorescence emission of RhB at 550 nm excited by 320 nm was greatly enhanced. The major overlap between the fluorescence excitation spectrum of RhB@MOF-5 (about 320 nm) and the ultraviolet absorption spectrum of PNPG (about 310 nm) lead to PNPG being a good IFE absorber in this sensing system. Under the optimized conditions, the excitation spectrum of the RhB@MOF-5 could be absorbed by PNPG, resulting in the dramatically decrease of fluorescence emission. After adding β-GCU into the system, the substrate of PNPG would be enzymatic hydrolyzed to *p*-nitrophenol (PNP) and glucose, then the IFE disappearance and the fluorescence recovered. The current sensing platform was interference-free and exhibited a broad linearity relationship for β-GCU range of 0.1–10 U L^{-1} (R^2 = 0.9957) with a limit of detection as low as 0.03 U L^{-1}, which was reduced by more than one orders compared with the reported methods. Moreover, the encapsulation of dyes using porous nanoparticles to achieve some tailor-made characteristics will enrich experimental design inspiration.

1. Introduction

β-Glucuronidase (β-GCU), a glycosidase mainly exists in cell membranes and extracellular matrices of tissues and organs [1,2], initiates the hydrolysis of glucopyranosyl glycoside from glycosaminoglycans to release glucose and the corresponding aglycone. The normal concentration level of serum β-GCU in human body is in the range of 3.48–5.72 U L^{-1}, whereas the disordering of β-GCU in human body is related to various diseases and even the development of cancers [3]. On the one hand, abnormal overexpression of β-GCU in serum is considered to be associated with malignant tumors, such as liver cancer [4], prostate cancer [5], gastric cancer [6], colon carcinoma [7] and especially tumors in necrotic regions [8]. On the other hand, underexpression of β-GCU in serum is related to hepatic failure and mucopolysaccharidosis [9,10]. Moreover, a series of physiological diseases, involving cholelithiasis [11], hepatic disorders [12] and epilepsy [13], are also related to abnormal serum β-GCU level. Hence, β-GCU has been taken as a significant tumor biomarker. So the detection of β-GCU activity is valuable in ascertaining and early-stage diagnosing cancer.

Of late years, great endeavors have been devoted to the development of efficient methods for the detection of β-GCU. A number of methods such as colorimetric methods and chemosensors have been developed [14–19]. Among them, method based on fluorescent probe, especially organic fluorescent probe, is an attractive strategy in terms of high sensitivity and selectivity. However, the organic fluorescent probes inevitably suffer from complicated synthesis, low photobleaching resistance, and high cytotoxicity [20–24]. In contrast, inorganic nanoprobes have become a powerful analytical strategy with remarkable advantages, such as simple synthesis process, excellent biocompatibility, high photobleaching resistance ability, and satisfactory dispersion in water [16,17,25,26]. Moreover, the present methods for the detection of β-GCU based on inorganic probes are still not

* Corresponding authors.
E-mail addresses: xialian01@163.com (L. Xia), fengliquhn@hotmail.com (F. Qu).

https://doi.org/10.1016/j.snb.2019.05.064
Received 19 March 2019; Received in revised form 15 May 2019; Accepted 17 May 2019
Available online 19 May 2019

sensitive or selective enough to monitoring β-GCU, which largely limited their practical applications in disease diagnosis. Thus, it is still challenging to develop methods for β-GCU detection with characteristics of high sensitivity and selectivity, as well as easily operation and excellent biocompatibility.

Metal organic frameworks (MOFs), rising as a fresh kind of meaningful microporous hybrid crystalline materials, are constructed by metal ions or metal clusters connecting with organic bridging ligands. On account of their attractive structures and superior physicochemical properties, including controlled sizes, uniform nanoscale cavities, and high surface areas, MOFs have exhibited wide utilizations in catalysis, gas storage, separation, drug delivery, bio-imaging and molecular recognition [27–34]. Additionally, their highly uniform nanoscale cavities, which act as micro-reactors, are conductive to concentrating targets in their pores, resulting in low detection limit and high sensing sensitivity [35]. Inner filter effect (IFE), a photophysical phenomenon, regulates fluorescence based on the absorption of the excitation or the emission light of fluorophores by absorbers in the sensing system [36–40]. In other words, IFE occurs when the absorption spectrum of the absorbers overlaps with the fluorescence excitation or emission spectrum of fluorophores. Because the substrate or the absorber neither require chemical link to the probe, nor require the special interaction with the probe, the sensing platforms based on IFE exhibit more simplicity when compared with sensors based on traditional fluorescence quenching mechanisms, such as fluorescence resonance energy transfer (FRET) and photo-induced electron transfer (PET) [41–43]. Nowadays, most of the reported probes based on MOFs are usually used for sensing metal ions, so that it is not only necessary but also very interesting to further expand the application of MOFs in bio-sensing. However, so far as we know, the MOFs-based probes via IFE for the detection of β-GCU activity with satisfactory sensitivity and selectivity have not been reported.

In this study, a hybrid nanocomposite of RhB@MOF-5 was constructed by embedding organic dye rhodamine B (RhB) into the porous crystalline Zn(II)-MOF via a facile one-pot synthesis approach. RhB@MOF-5 aqueous solution owns a yellow-green emission of RhB at 552 nm with the excitation wavelength at 315 nm. Moreover, we found that the absorption spectrum of PNPG, a substrate of β-GCU, could overlap with the excitation spectrum of the RhB@MOF-5. Based on these properties, we rationally designed a “turn on” fluorescence sensor by employing RhB@MOF-5 as nanoprobe and the PNPG as substrate to detect β-GCU based on the synergistic action of IFE and static quenching effect (SQE) (Scheme 1). Benefit from the gathering effect of MOF-5, the improvement of fluorescent properties of RhB in RhB@MOF-5, as well as the special recognition of PNPG substrate based on IFE, a highly sensitive and selective method for monitoring β-GCU in human serum was developed. Using the developed method, an assay was performed to detect β-GCU in human serum of both healthy and cancer people, the results were satisfactory.

2. Experimental section

2.1. Materials and reagents

4-Nitrophenyl-β-D-glucuronide (PNPG), *p*-nitrophenol (PNP) and β-glucuronidase (β-GCU, 110 units/g) from Helix pomatia were purchased from Sigma-Aldrich (Steinheim, Germany). Rhodamine B (RhB), 1, 4-benzenedicarboxylic acid (BDC), sodium hydroxide (NaOH), L-alanine (L-Ala), L-tyrosine (L-Tyr), DL-phenylalanine (DL-Phe), L-tryptophan (L-Try), L-valine (L-Val), L-serine (L-Ser), L-cysteine (L-Cys), homocysteine (Hcy), L-glutathione (GSH), glucose (Glu), ascorbic acid (AA), adenosine triphosphate (ATP), adenosine monophosphate (AMP), guanosine triphosphate (GTP), glucose oxidase (GOD) and alkaline phosphatase (ALP) were obtained from Aladdin Chemical Reagent Co. Ltd. (Shanghai, China). Metal salts (CH_3COONa, KCl, $MnCl_2{\cdot}4H_2O$, $Ni(NO_3)_2{\cdot}6H_2O$, $CaCl_2$, $Co(CH_3COO)_2$, $MgCl_2{\cdot}6H_2O$, $FeSO_4{\cdot}7H_2O$, $BaCl_2{\cdot}2H_2O$, $Pb(NO_3)_2$, $HgCl_2$, $ZnCl_2$, $AlCl_3{\cdot}6H_2O$, $FeCl_3{\cdot}6H_2O$ and $CrCl_3{\cdot}6H_2O$) were supplied by Fuyu Chemical Reagent Co. (Tianjin, China). N, N-Dimethylformamide (DMF) and acetic acid (HAc) were brought from Beijing Chemical Reagent Co. Ltd. (Beijing, China). And all other reagents and solvents of analytical grade were commercially available and used as received without purification.

2.2. Synthesis of MOF-5 and RhB@MOF-5 composites

The detailed information for preparing of MOF-5 and RhB@MOF-5 composites were presented in Supporting Information.

2.3. Fluorescence quenching assay for PNPG

Assay for incubation time: 100 μL PNPG (the final concentration was 0.5 mmol L^{-1}) was added into 100 μL of RhB@MOF-5 solution (60 mg L^{-1}) with 800 μL of NaAC-HAc buffer (100 mmol L^{-1}, pH 5.0). After different incubation times, the fluorescence emission spectra of the mixture were recorded respectively.

Assay for PNPG concentration: 100 μL of RhB@MOF-5 composites (60 mg L^{-1}), 800 μL of NaAC-HAc buffer (100 mmol L^{-1}, pH 5.0) and 100 μL of varied concentrations of PNPG ranging from 0.1 to 1 mmol L^{-1} were mixed, after incubation for certain time, the fluorescent spectra of the mixture were measured.

2.4. β-GCU detection

Fluorescence assay for β-GCU was conducted as the following procedures. 100 μL β-GCU with various concentrations was added to NaAC-HAc buffer (100 mmol L^{-1}, pH 5.0) containing RhB@MOF-5 composites (60 mg L^{-1}), AA (1 mmol L^{-1}) and PNPG (0.2 mmol L^{-1}), then adjusted the total volume to 700 μL. After incubation for 30 min at 37 °C, the mixed solution was adjusted to alkaline by adding 300 μL NaOH solution (0.01 mol L^{-1}) and recorded the fluorescence emission spectra using excitation wavelength of 315 nm. The selectivity of this sensing system for β-GCU was investigated by using other biomolecules or common ions (including Na^+, K^+, Mn^{2+}, Ni^{2+}, Ca^{2+}, Co^{2+}, Mg^{2+}, Fe^{2+}, Ba^{2+}, Pb^{2+}, Hg^{2+}, Zn^{2+}, Al^{3+}, Fe^{3+}, Cr^{3+}, L-Ala, L-Tyr, DL-Phe, L-Try, L-Val, L-Ser, L-Cys, Hcy, GSH, Glu, AA, ATP, AMP, GTP, GOD and ALP) instead of β-GCU.

2.5. Analysis of β-GCU in human serum samples

The above platform was used to the direct analysis of β-GCU in human serum which were obtained from two healthy samples and two cancer samples donated by the First Hospital of Qufu (Shandong, China), and the authors declared that all studies were performed in compliance with the relevant laws and institutional guidelines. During the analysis of real samples, 100 μL human serums were added to take the place of the standard β-GCU solution, and other procedures should follow the above β-GCU assay.

2.6. Characterization methods

All the used instruments were demonstrated in Supporting Information.

3. Results and discussion

3.1. Sensing mechanism and the characterization of RhB@MOF-5 composites

The preparation methods and the luminescent mechanism of the sensing platform were shown in Scheme 1. In order to better understand the fluorescent properties of the as-prepared RhB@MOF-5 composite, its fluorescence spectra were recorded (Fig. S1). The fluorescence

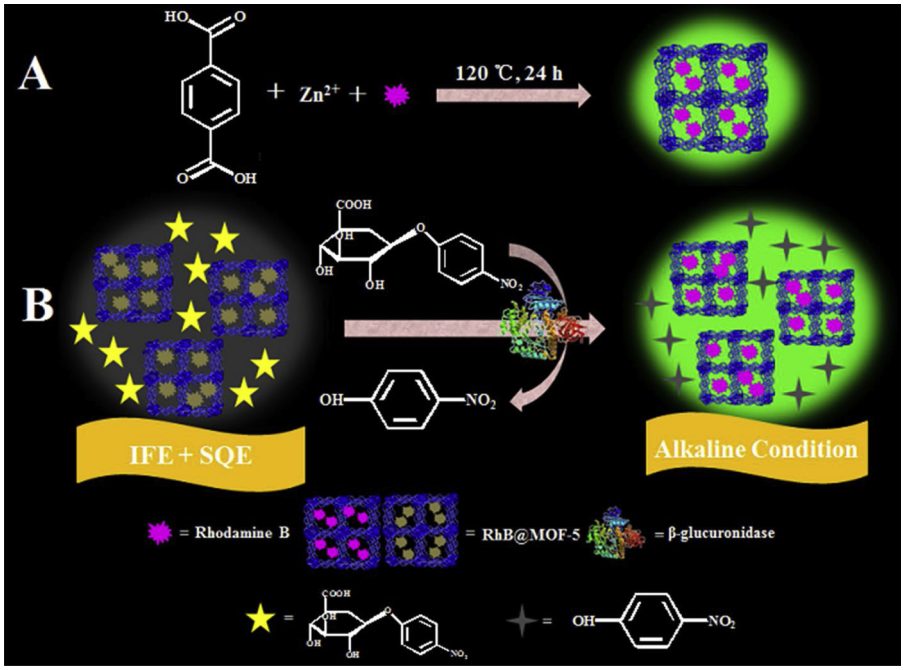

Scheme 1. (A) The preparation procedure of RhB@MOF-5 by one-pot synthesis approach. (B) The mechanism for β-GCU detection based on the synergistic effect of IFE and SQE (IFE: inner filter effect; SQE: static quenching effect).

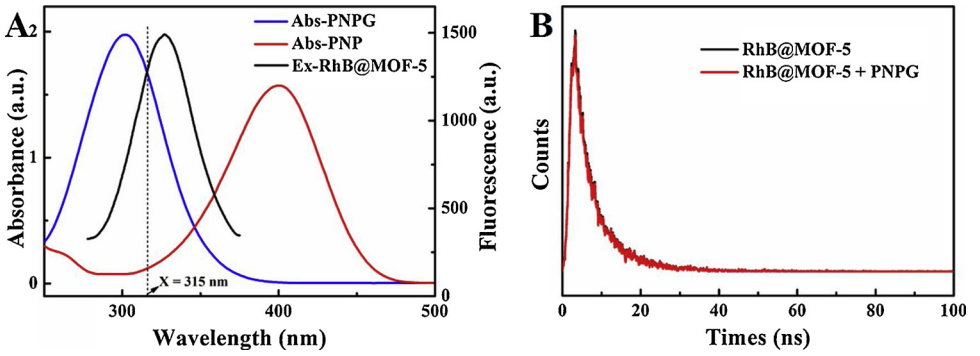

Fig. 1. (A) The UV–vis absorption spectra of PNPG (blue line) and PNP (red line), the fluorescence excitation spectrum of RhB@MOF-5 (black line). (B) The fluorescence decay curves of RhB@MOF-5 in the absence and presence of PNPG (For interpretation of the references to colour in this figure legend, the reader is referred to the web version of this article.).

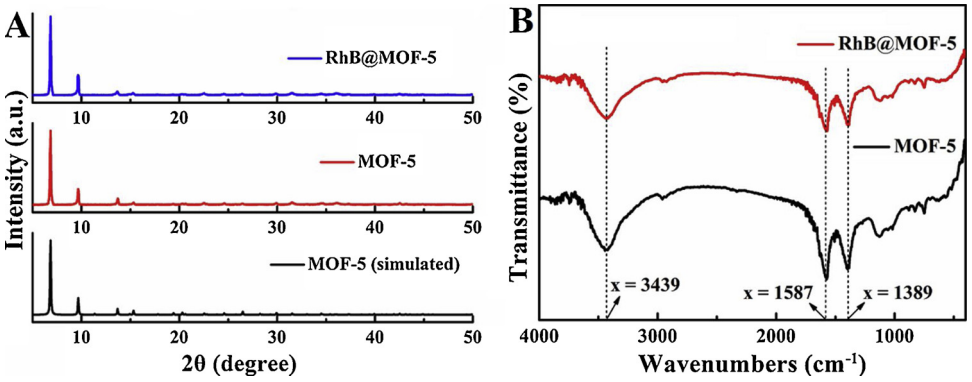

Fig. 2. (A) XRD images of the simulated MOF-5 (black), the as-prepared MOF-5 (red) and RhB@MOF-5 (blue). (B) FT-IR spectrum of MOF-5 (black) and RhB@MOF-5 (red) (For interpretation of the references to colour in this figure legend, the reader is referred to the web version of this article.).

excitation spectrum displayed a strong peak at about 320 nm, and a strong fluorescence emission peak at 550 nm under this excitation wavelength was observed correspondingly. Furthermore, the inset in Fig. S1B depicted the photograph of RhB@MOF-5 solution, which was obtained under UV light (365 nm). To verify the IFE mechanism for the β-GCU detection, the spectroscopic properties of PNPG and PNP were also studied. As shown in Fig. 1A, the maximum fluorescence excitation of RhB@MOF-5 was at about 320 nm, and the maximum ultraviolet absorption of PNPG was at approximately 310 nm, thus there was a major overlap between them, indicating that PNPG could be a good IFE absorber in RhB@MOF-5 system. Specially, the UV–vis absorption peak of PNP (the hydrolysis product of PNPG by β-GCU) was at about 400 nm under alkaline condition, which had no effect on the fluorescence emission of RhB@MOF-5 (Fig. S2). Therefore, the PNPG acted not only

as the IFE absorber, but also as the substrate of the β-GCU. For further studying the mechanism of fluorescence quenching, time-resolved fluorescence spectra of RhB@MOF-5 in the absence and presence of PNPG were measured. As shown in Fig. 1B, the fluorescence lifetime of RhB@MOF-5 (about 5.6 ns) remained constant after adding PNPG, which demonstrated that the fluorescence quenching of RhB@MOF-5 by PNPG may also obey a SQE [44,45]. Therefore, both the IFE and SQE mechanism may be responsible for the fluorescence suppression of RhB@MOF-5 caused by PNPG.

In order to verify the successful preparation of RhB@MOF-5 composite, it was firstly characterized by X-ray diffraction (XRD). As depicted in Fig. 2A, the XRD patterns of the prepared MOF-5 and RhB@MOF-5 were highly consistent with that of the simulated ones, indicating the successful preparation of the materials and the negligible influence of the encapsulated RhB on the lattice of MOF-5. Additionally, the high similarity of XRD peaks between MOF-5 and RhB@MOF-5 demonstrated that the RhB molecules were encapsulated into the pores of MOF-5 particle, rather than physically adsorbed on the surface of particle [46]. The fourier transform-infrared (FT-IR) spectra of MOF-5 and RhB@MOF-5 composites were showed in Fig. 2B. The peak located at 3439 cm^{-1} was ascribed to the O—H stretching vibration [47]. The strong peaks from MOF-5 nanocrystals at 1389 cm^{-1} and 1587 cm^{-1}, originated from the symmetrical stretching vibration and the asymmetric stretching vibration of carboxylate, had no blue or red shift after encapsulation of RhB, suggesting that RhB in the composite had no influence on the structure of the MOF-5. Furthermore, the peaks of RhB at 1590, 1179, 1342 and 1645 cm^{-1} were not observed after its capsulation into MOF-5, further suggesting that RhB molecules were localized inside the pores of MOF-5 [48]. Scanning electron microscopy (SEM) observation (Fig. S3) clearly described the “cube-sugar-like” morphology of the obtained MOF-5 and RhB@MOF-5 composites. What’s more, the average side-length of the prepared material was about 1.3 μm, and the RhB@MOF-5 was uniform crystals decorated with a few of nanoscale sub-crystals.

3.2. Optimization of the detection condition

Several factors that might affect the method sensitivity were optimized, including the incubation time of PNPG with RhB@MOF-5 and the concentration of PNPG. As shown in Fig. S4, after adding PNPG, the fluorescence emission of the RhB@MOF-5 suspension decreased rapidly and gradually reached equilibrium at 2 min. As for the amount of PNPG, when various concentrations of PNPG (0.1 mmol L^{-1}, 0.2 mmol L^{-1}, 0.3 mmol L^{-1}, 0.4 mmol L^{-1}, 0.5 mmol L^{-1}, 0.6 mmol L^{-1}, 0.7 mmol L^{-1}, 0.8 mmol L^{-1}, 0.9 mmol L^{-1} and 1.0 mmol L^{-1}) were added to the RhB@MOF-5 dispersive solution, the fluorescence intensity was decreased gradually with the increasing the PNPG amount. When the concentration of PNPG was up to 0.5 mmol L^{-1}, 94.18% fluorescence of RhB@MOF-5 was quenched, whereas further increase the PNPG amount, no obviously change of quenching effect observed (Fig. 3A). In addition, the sensitivity of β-GCU (10 U L^{-1}) response to PNPG towards different concentrations (0.1-0.5 mmol L^{-1}) was also investigated, and the results were shown in Fig. 3B. From the Fig. 3B, we could see that the maximum fluorescence recovery was achieved when the PNPG concentration was below 0.2 mmol L^{-1}. Although the highest quenching efficiency was achieved at the PNPG concentration of 0.5 mmol L^{-1}, 0.2 mmol L^{-1} PNPG can also achieve satisfactory quenching effect (88.71%). Considering that high PNPG concentration could yield better quenching efficiency, whereas the excess PNPG could lead to low sensitivity to β-GCU, the PNPG concentration of 0.2 mmol L^{-1} was selected as the optimal PNPG concentration in the following experiments.

3.3. Performance of β-GCU activity assay

In order to obtain the best response effect, the main conditions possible to influence the sensitivity of β-GCU detection, including reaction time, pH values and temperature were optimized in detail. As shown in Fig. S5, time of 30 min, pH of 5.0 and temperature of 37 °C were chosen as the optimum detection conditions. Based on the above requirements, the fluorescence emission intensity of RhB@MOF-5/PNPG changes were recorded after introducing a series of concentrations of β-GCU from 0.1 to 10 U L^{-1} (Fig. 4A). It was clear that the fluorescence increased gradually with the increase of β-GCU concentration. What’s more, a good linear relationship ($F = 764.89 + 55.20c$, $R^2 = 0.9957$) between the fluorescence intensity and β-GCU concentration was achieved (Fig. 4B). The limit of detection (LOD) was calculated to be 0.03 U L^{-1} via 3SD/S (SD is the standard deviation of the blank samples and S is the slope of the linear calibration plot), which decreased by over two orders when compared to the normal levels of β-GCU in human serum (3.48–5.72 U L^{-1}). Therefore, the ultra-sensitivity of this β-GCU detection platform is highly competent to detect β-GCU in biological samples. Furthermore, performance of our method were compared with the previously reported methods in detecting β-GCU (Table S1), and the LOD of the proposed probe is much lower than that of the most reported sensors.

3.4. Selectivity of IFE based sensing platform

To investigate the specificity of the RhB@MOF-5/PNPG nanosensor platform toward β-GCU, the potential interferences in human serum samples, containing various metal cations (Na^+, K^+, Mn^{2+}, Ni^{2+}, Ca^{2+}, Co^{2+}, Mg^{2+}, Fe^{2+}, Ba^{2+}, Pb^{2+}, Hg^{2+}, Zn^{2+}, Al^{3+}, Fe^{3+} and Cr^{3+}), amino acids (L-Ala, L-Tyr, DL-Phe, L-Try, L-Val, L-Ser, L-Cys, Hcy and GSH) and other potential biological interferences (Glu, AA, ATP, AMP, GTP, GOD and ALP) were explored under the conditions same as that of the β-GCU (Fig. 5). It is known that Fe^{3+} has the similar ultraviolet absorption spectrum to PNPG, so it could lead to fluorescence quenching at a certain extent (Fig. S6A). Interestingly, neither AA nor Fe^{2+} has effect on the fluorescence of RhB@MOF-5 (Fig. S6B) so that we could use AA to reduce Fe^{3+} to Fe^{2+} to ensure its selectivity (Fig. S7). The experimental results in Fig. 5 demonstrated that only the

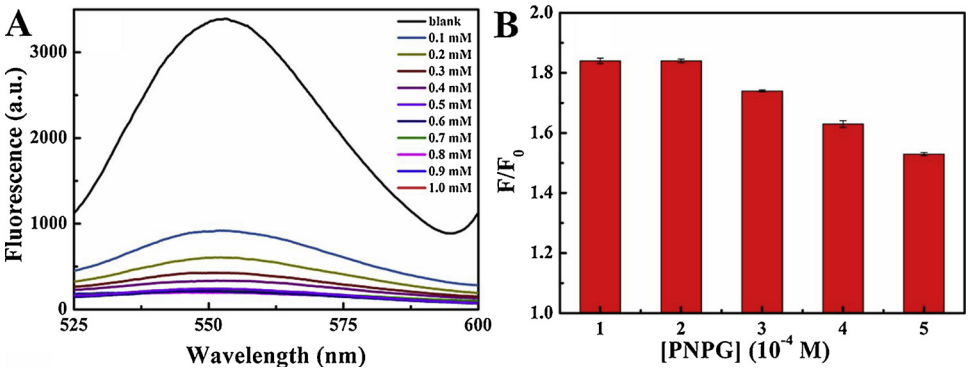

Fig. 3. (A) Fluorescence emission spectra of RhB@MOF-5 in the presence of varying concentrations of PNPG (0.1 mmol L^{-1}, 0.2 mmol L^{-1}, 0.3 mmol L^{-1}, 0.4 mmol L^{-1}, 0.5 mmol L^{-1}, 0.6 mmol L^{-1}, 0.7 mmol L^{-1}, 0.8 mmol L^{-1}, 0.9 mmol L^{-1} and 1.0 mmol L^{-1}). (B) The sensitivity of β-GCU (10 U L^{-1}) response to different concentrations of PNPG (0.1 mmol L^{-1}, 0.2 mmol L^{-1}, 0.3 mmol L^{-1}, 0.4 mmol L^{-1} and 0.5 mmol L^{-1}). (F_0 and F are the fluorescence intensities of RhB@MOF-5/PNPG in the absence and presence of β-GCU, respectively).

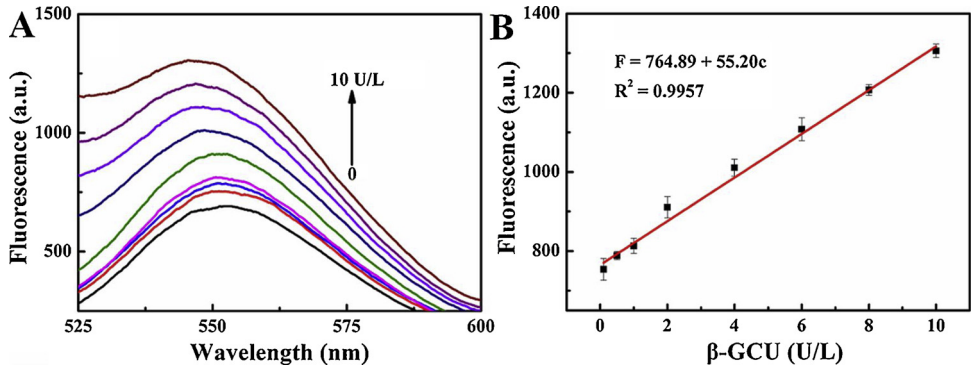

Fig. 4. (A) Fluorescence emission spectra of the RhB@MOF-5/PNPG upon the addition of various concentrations of β-GCU from 0 to 10 U L^{-1} in the presence of AA (1 mmol L^{-1}). (B) Relationship between the fluorescence intensity and the concentration of β-GCU.

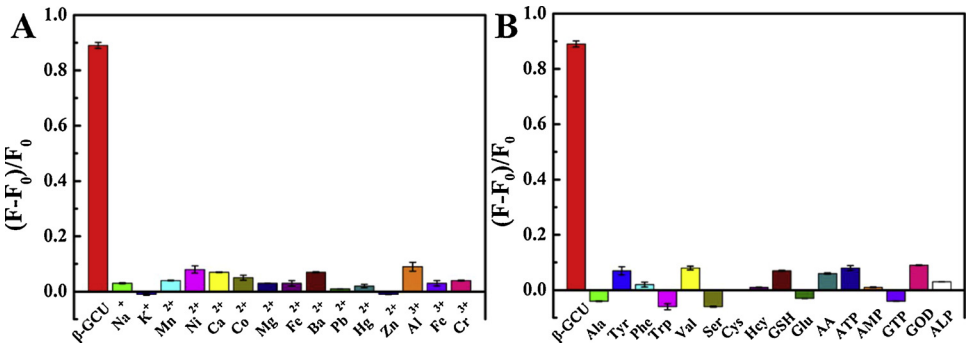

Fig. 5. (A) Fluorescence intensity response ($(F-F_0)/F_0$) of RhB@MOF-5/PNPG toward various metal ions in the presence of AA (β-GCU, 10 U L^{-1}; Fe^{3+}, 10^{-4} mol L^{-1}; AA, 10^{-3} mol L^{-1}; metal ions, 10^{-3} mol L^{-1}). (B) Fluorescence intensity response ($(F-F_0)/F_0$) of the RhB@MOF-5/PNPG toward various amino acids and other potential biological interferences in the presence of AA (β-GCU, 10 U L^{-1}; L-Ala, L-Tyr, DL-Phe, L-Try, L-Val, L-Ser, L-Cys, Hcy, GSH, Glu, AA, ATP, AMP and GTP, 10^{-3} mol L^{-1}; GOD and ALP, 10 U L^{-1}; AA, 10^{-3} mol L^{-1}). Where F_0 and F are fluorescence intensities of the RhB@MOF-5/PNPG in the absence and presence of various substances, respectively.

target of β-GCU led to obvious fluorescence recovery in the presence of AA, while the other substances had negligible effect on the fluorescent recovery, indicating that this RhB@MOF-5/PNPG nanosensor was highly specific for the β-GCU detection.

3.5. Detection of β-GCU in human serum samples

To demonstrate the potential practical application of the offered sensor in complex biological samples, an assay was performed to detect β-GCU in human serum of both healthy and cancer people. These samples were added with three different concentrations and analyzed using the same method to evaluate the recovery. The results in Table S2 showed that the recoveries of β-GCU in serum samples were in the range of 98.39%–104.57% with the RSDs less than 5%, indicating the high analytical accuracy and precision of the proposed method. Therefore, this nanosensor platform could be potentially applied for β-GCU detection assay in practical application. Moreover, as shown in Table S2, the concentrations of β-GCU in the cancer patients' serum (˜13 U L^{-1}) were much higher than that of in healthy adults (˜5 U L^{-1}). The above results further confirmed that the β-GCU concentration was closely related with cancers so that it could act as a significative cancer biomarker.

4. Conclusion

In summary, a composite of RhB@MOF-5 was rationally designed and successfully applied for the "turn on" fluorescence detection of β-GCU using PNPG as the spectra absorber and substrate based on the synergistic effect of IFE and SQE mechanism. Owing to the capsulation of RhB into MOF-5, the best excitation wavelength of RhB to the emission spectrum at 550 nm blue shifted to 315 nm, leading to large stocks shift. By tuning the absorption and non-absorption of spectrum at 315 nm with adding the PNPG and β-GCU, high on-off-on fluorescence changes were observed and resulted to the highly sensitive response to the target of β-GCU. Using this detection platform, a good linear relationship for β-GCU detection from 0.1 to 10 U L^{-1} (R^2 = 0.9957) was achieved, and the LOD was as low as 0.03 U L^{-1}, which was reduced by more than one orders when compared with the reported methods. Moreover, this established sensing platform was successfully applied for the determination of β-GCU in human serum samples with satisfactory results. Importantly, the strategy of encapsulation of dyes using porous nanoparticles to achieve some tailor-made characteristics used in this study will enrich experimental design inspiration.

Declaration of interest

The authors declare that there are no conflicts of interest.

Acknowledgements

This work is supported by the National Natural Science Foundation of China (No. 21505084, 21775089, 21475074), Key Research and Development Program of Shandong Province (No. 2017GSF19109), the Innovation Project of Shandong Graduate Education (No. SDYY16091) and Natural Science Foundation Projects of Shandong Province (ZR2014BM029).

Appendix A. Supplementary data

Supplementary material related to this article can be found, in the online version, at doi:https://doi.org/10.1016/j.snb.2019.05.064.

References

[1] Y.Z. Jin, X.G. Tian, L.L. Jin, Y.L. Cui, T. Liu, Z.L. Yu, X.K. Huo, J.N. Cui, C.P. Sun, C. Wang, J. Ning, B.J. Zhang, L. Feng, X.C. Ma, Highly specific near-infrared fluorescent probe for the real-time detection of β-glucuronidase in various living cells and animals, Anal. Chem. 90 (2018) 3276–3283.
[2] A.R. Ronald, F. Silverblatt, H. Clark, R.E. Cutler, M. Turck, Failure of urinary beta-

glucuronidase activity to localize the site of urinary tract infection, Appl. Microbiol. 21 (1971) 990–992.
[3] B. Sperker, J.T. Backman, H.K. Kroemer, The role of β-glucuronidase in drug disposition and drug targeting in humans, Clin. Pharmacokinet. 33 (1997) 18–31.
[4] T.C. Cheng, S.R. Roffler, S.C. Tzou, K.H. Chuang, Y.C. Su, C.H. Chuang, C.H. Kao, C.S. Chen, I.H. Harn, K.Y. Liu, T.L. Cheng, Y.L. Leu, An activity-based near-infrared glucuronide trapping probe for imaging β-glucuronidase expression in deep tissues, J. Am. Chem. Soc. 134 (2012) 3103–3110.
[5] Y.Y. Di, S.P. Ji, P. Wolf, E.S. Krol, J. Alcorn, Enterolactone glucuronide and β-glucuronidase in antibody directed enzyme prodrug therapy for targeted prostate cancer cell treatment, AAPS Pharm. Sci. Tech. 18 (2017) 2336–2345.
[6] K. Bosslet, R. Straub, M. Blumrich, J. Czech, M. Gerken, B. Sperker, H.K. Kroemer, J.P. Gesson, M. Koch, C. Monneret, Elucidation of the mechanism enabling tumor selective prodrug monotherapy, Cancer Res. 58 (1998) 1195–1201.
[7] N. Waszkiewicz, S.D. Szajda, E. Konarzewska-Duchnowska, B. Zalewska-Szajda, R. Gałązkowski, A. Sawko, H. Nammous, V. Buko, A. Szulc, K. Zwierz, J. Ladny, Serum β-glucuronidase as a potential colon cancer marker: a preliminary study, Postepy Hig. Med. Dosw. 69 (2015) 436–439.
[8] P.H.J. Houba, E. Boven, C.A.M. Erkelens, R.G.G. Leenders, J.W. Scheeren, H.M. Pinedo, H.J. Haisma, The efficacy of the anthracycline prodrug daunorubicin-GA3 in human ovarian cancer xenografts, Br. J. Cancer 78 (1998) 1600–1606.
[9] H. Ohta, Measurement of serum immunoreactive beta-glucuronidase: a possible serological marker for histological hepatic cell necrosis and to predict the histological progression of hepatitis, Hokkaido Igaku Zasshi 66 (1991) 545–557.
[10] M.K. Parente, R. Rozen, S.H. Seeholzer, J.H. Wolfe, Integrated analysis of proteome and transcriptome changes in the mucopolysaccharidosis type VII mouse hippocampus, Mol. Genet. Metab. 118 (2016) 41–54.
[11] H.W. Lee, M.K. Choo, E.A. Bae, D.H. Kim, β-Glucuronidase inhibitor tectorigenin isolated from the flower of Pueraria thunbergiana protects carbon tetrachloride-induced liver injury, Liver Int. 23 (2003) 221–226.
[12] M. Taha, N.H. Ismail, S. Imran, F. Rahim, A. Wadood, H. Khan, H. Ullah, U. Salar, K.M. Khan, Synthesis, β-glucuronidase inhibition and molecular docking studies of hybrid bisindole-thiosemicarbazides analogs, Bioorg. Chem. 68 (2016) 56–63.
[13] M. Taha, N.H. Ismail, W. Jamil, K.M. Khan, U. Salar, S.M. Kashif, F. Rahim, Y. Latif, Synthesis and evaluation of unsymmetrical heterocyclic thioureas as potent β-glucuronidase inhibitors, Med. Chem. Res. 24 (2015) 3166–3173.
[14] C.B. Burghina, B. Heery, F. Regan, Continuous fluorometric method for measuring β-glucuronidase activity: comparative analysis of three fluorogenic substrates, Analyst 140 (2015) 5953–5964.
[15] X.K. Huo, X.G. Tian, Y.N. Li, L. Feng, Y.L. Cui, C. Wang, J.N. Cui, C.P. Sun, K.X. Liu, X.C. Ma, A highly selective ratiometric fluorescent probe for real-time imaging of β-glucuronidase in living cells and zebrafish, Sens. Actuator B-Chem. 262 (2018) 508–515.
[16] S.M. Lu, G.L. Li, Z.X. Lv, N.N. Qiu, W.H. Kong, P.W. Gong, G. Chen, L. Xia, X.X. Guo, J.M. You, Y.N. Wu, Facile and ultrasensitive fluorescence sensor platform for tumor invasive biomarker β-glucuronidase detection and inhibitor evaluation with carbon quantum dots based on inner-filter effect, Biosens. Bioelectron. 85 (2016) 358–362.
[17] D.D. Tang, J.Y. Zhang, X.D. Hou, P. Wu, Phosphorescent inner filter effect-based sensing system for determination of β-glucuronidase using manganese-doped zinc sulfide quantum dots, Chin. J. Anal. Chem. 45 (2017) 1909–1914.
[18] L. Wu, X. Qu, Cancer biomarker detection: recent achievements and challenges, Chem. Soc. Rev. 44 (2015) 2963–2997.
[19] P.W. Gong, L. Sun, F. Wang, X.C. Liu, Z.Q. Yan, M.Z. Wang, L. Zhang, Z.Z. Tian, Z. Liu, J.M. You, Highly fluorescent N-doped carbon dots with two-photon emission for ultrasensitive detection of tumor marker and visual monitor anticancer drug loading and delivery, Chem. Eng. J. 356 (2019) 994–1002.
[20] L. Feng, Y.L. Yang, X.K. Huo, X.G. Tian, Y.J. Feng, H.W. Yuan, L.J. Zhao, C. Wang, P. Chu, F.D. Long, W. Wang, X.C. Ma, Highly selective NIR probe for intestinal β-glucuronidase and high-throughput screening inhibitors to therapy intestinal damage, ACS Sens. 3 (9) (2018) 1727–1734.
[21] K. Dou, Q. Fu, G. Chen, F.B. Yu, Y.X. Liu, Z.P. Cao, G.L. Li, X.E. Zhao, L. Xia, L.X. Chen, H. Wang, J.M. You, A novel dual-ratiometric-response fluorescent probe for SO_2/ClO^- detection in cells and in vivo and its application in exploring the dichotomous role of SO_2 under the ClO^- induced oxidative stress, Biomaterials 133 (2017) 82–93.
[22] H.L. Guo, G. Chen, M. Gao, R. Wang, Y.X. Liu, F.B. Yu, Imaging of endogenous hydrogen peroxide during the process of cell mitosis and mouse brain development with a near-infrared ratiometric fluorescent probe, Anal. Chem. 91 (2019) 1203–1210.
[23] J. Ning, T. Liu, P.P. Dong, W. Wang, G.B. Ge, B. Wang, Z.L. Yu, L. Shi, X.G. Tian, X.K. Huo, L. Feng, C. Wang, C.P. Sun, J.N. Cui, T.D. James, X.C. Ma, Molecular design strategy to construct the near-infrared fluorescent probe for selectively sensing human cytochrome P450 2J2, J. Am. Chem. Soc. 141 (2019) 1126–1134.
[24] K. Dou, G. Chen, F.B. Yu, Y.X. Liu, L.X. Chen, Z.P. Cao, T. Chen, Y.L. Li, J.M. You, Bright and sensitive ratiometric fluorescent probe enabling endogenous FA imaging and mechanistic exploration of indirect oxidative damage due to FA in various living systems, Chem. Sci. 8 (2017) 7851–7861.
[25] F.L. Qu, H.M. Pei, R.M. Kong, S.Y. Zhu, L. Xia, Novel turn-on fluorescent detection of alkaline phosphatase based on green synthesized carbon dots and MnO_2 nanosheets, Talanta 165 (2017) 136–142.
[26] H.M. Pei, Y.Q. Zheng, R.M. Kong, L. Xia, F.L. Qu, Niche nanoparticle-based FRET assay for bleomycin detection via DNA scission, Biosens. Bioelectron. 85 (2016) 76–82.
[27] J.Y. Zheng, X.L. Cui, Q.W. Yang, Q.L. Ren, Y.W. Yang, H.B. Xing, Shaping of ultrahigh-loading MOF pellet with a strongly anti-tearing binder for gas separation and storage, Chem. Eng. J. 354 (2018) 1075–1082.
[28] X.F. Qiao, Y.B. Yan, D. Tian, Z.C. Yang, J.L. Li, S.T. Zhao, MOF matrix doped with rare earth ions to realize ratiometric fluorescent sensing of 2,4,6-trinitrophenol: synthesis, characterization and performance, Sens. Actuator B-Chem. 286 (2019) 1–8.
[29] J.W. Liu, Y. Zhang, X.W. Chen, J.H. Wang, Graphene oxide are earth metal-organic framework composites for the selective isolation of hemoglobin, ACS Appl. Mater. Inter. 6 (2014) 10196–10204.
[30] Z.M. He, Y.L. Dai, X.L. Li, D. Guo, Y.J. Liu, X.L. Huang, J.J. Jiang, S. Wang, G.Z. Zhu, F.W. Zhang, L.S. Lin, J.J. Zhu, G.C. Yu, X.Y. Chen, Hybrid nanomedicine fabricated from photosensitizer-terminated metal-organic framework nanoparticles for photodynamic therapy and hypoxia-activated cascade chemotherapy, Small 15 (2019) 1804131.
[31] C. Yang, K. Chen, M. Chen, X.X. Hu, S.Y. Huan, L.L. Chen, G.S. Song, X.B. Zhang, Nanoscale metal-organic framework based two-photon sensing platform for bioimaging in live tissue, Anal. Chem. 91 (2019) 2727–2733.
[32] J.A. Gustafson, C.E. Wilmer, Optimizing information content in MOF sensor arrays for analyzing methane-air mixtures, Sens. Actuator B-Chem. 267 (2018) 483–493.
[33] C.D. Wu, A. Hu, L. Zhang, W. Lin, A homochiral porous metal-organic framework for highly enantioselective heterogeneous asymmetric catalysis, J. Am. Chem. Soc. 127 (2005) 8940–8941.
[34] J. Zhou, X. Li, L.L. Yang, S.L. Yan, M.M. Wang, D. Cheng, Q. Chen, Y.L. Dong, P. Liu, W.Q. Cai, C.C. Zhang, The Cu-MOF-199/single-walled carbon nanotubes modified electrode for simultaneous determination of hydroquinone and catechol with extended linear ranges and lower detection limits, Anal. Chim. Acta 899 (2015) 57–65.
[35] Y. Ma, H. Su, X. Kuang, X. Li, T. Zhang, B. Tang, Heterogeneous nano metal-organic framework fluorescence probe for highly selective and sensitive detection of hydrogen sulfide in living cells, Anal. Chem. 86 (2014) 11459–11463.
[36] A.S. Tanwar, L.R. Adil, M.A. Afroz, P.K. Iyer, Inner filter effect and resonance energy transfer based attogram level detection of nitroexplosive picric acid using dual emitting cationic conjugated polyfluorene, ACS Sens. 3 (2018) 1451–1461.
[37] G.M. Khairy, A. Duerkop, Dipsticks and sensor microtiterplate for determination of copper (II) in drinking water using reflectometric RGB readout of digital images, fluorescence or eye-vision, Sens. Actuator B-Chem. 281 (2019) 878–884.
[38] Q. Long, A.J. Fang, Y.Q. Wen, H.T. Li, Y.Y. Zhang, S.Z. Yao, Rapid and highly-sensitive uric acid sensing based on enzymatic catalysis-induced upconversion inner filter effect, Biosens. Bioelectron. 86 (2016) 109–114.
[39] Q. Lin, X. Yan, Q. Lai, X.G. Su, Bimetallic gold/silver nanoclusters-gold nanoparticles based fluorescent sensing platform via the inner filter effect for hyaluronidase activity detection, Sens. Actuator B-Chem. 282 (2019) 45–51.
[40] M. Zheng, Z.G. Xie, D. Qu, D. Li, P. Du, X.B. Jing, Z.C. Sun, On-off-on fluorescent carbon dot nanosensor for recognition of chromium (VI) and ascorbic acid based on the inner filter effect, ACS Appl. Mater. Inter. 5 (2013) 13242–13247.
[41] C.T. He, Z.J. Liu, Q.L. Wu, J. Zhao, R.Y. Liu, B.H. Liu, T.T. Zhao, Ratiometric fluorescent biosensor for visual discrimination of cancer cells with different telomerase expression levels, ACS Sens. 3 (2018) 757–762.
[42] B. Daly, J. Ling, A.P.D. Silva, Current developments in fluorescent PET (photo-induced electron transfer) sensors and switches, Chem. Soc. Rev. 44 (2015) 4203–4211.
[43] S. Yang, C.C. Guo, Y. Li, J.R. Guo, J. Xiao, Z.H. Qing, J.S. Li, R.H. Yang, A ratiometric two-photon fluorescent cysteine probe with well-resolved dual emissions based on intramolecular charge transfer-mediated two-photon-FRET integration mechanism, ACS Sens. 3 (2018) 2415–2422.
[44] P.F. Shen, Y.S. Xia, Synthesis-modification integration: one-step fabrication of boronic acid functionalized carbon dots for fluorescent blood sugar sensing, Anal. Chem. 86 (2014) 5323–5329.
[45] X.H. Zhu, T.B. Zhao, Z. Nie, Y. Liu, S.Z. Yao, Non-redox modulated fluorescence strategy for sensitive and selective ascorbic acid detection with highly photoluminescent nitrogen-doped carbon nanoparticles via solid-state synthesis, Anal. Chem. 87 (2015) 8524–8530.
[46] J.J. Deng, K. Wang, M. Wang, P. Yu, L.Q. Mao, Mitochondria targeted nanoscale zeolitic imidazole framework-90 for ATP imaging in live cells, J. Am. Chem. Soc. 139 (2017) 5877–5882.
[47] Y. Hu, T. Guo, X. Ye, Q. Li, M. Guo, H. Liu, Z. Wu, Dye adsorption by resins: effect of ionic strength on hydrophobic and electrostatic interactions, Chem. Eng. J. 228 (2013) 392–397.
[48] X.F. Lyu, Y.F. Zhang, R.N. Zare, J. Ge, Z. Liu, One-pot synthesis of protein-embedded metal-organic frameworks with enhanced biological activities, Nanosci. Nanotechnol. Lett. 14 (2014) 5761–5765.